Available online at www.sciencedirect.com
ScienceDirect
European Journal of Mechanics B/Fluids 25 (2006) 987–1007

Wave propagation in a fluid flowing through a curved thin-walled elastic tube

Giuseppe Pontrelli [a,*], Amabile Tatone [b]

[a] *Istituto per le Applicazioni del Calcolo – CNR Viale del Policlinico, 137-00161 Roma, Italy*
[b] *DISAT, Facoltà di Ingegneria, Università dell'Aquila, 67040 Monteluco di Roio (AQ), Italy*

Received 22 October 2004; received in revised form 20 July 2005; accepted 6 December 2005

Available online 9 February 2006

Abstract

The pulsatile flow in a curved elastic pipe of circular cross section is investigated. The unsteady flow of a viscous fluid and the wall motion equations are written in a toroidal coordinate system, superimposed and linearized over a steady state solution. Being the main application relative to the vascular system, the radius of the pipe is assumed small compared with the radius of curvature. This allows an asymptotic analysis over the curvature parameter. The model results an extension of the Womersley's model for the straight elastic tube. A numerical solution is found for the first order approximation and computational results are finally presented, demonstrating the role of curvature in the wave propagation and in the development of a secondary flow.

Keywords: Curved elastic tubes; Arterial flow; Perturbation methods; Numerical methods

1. Introduction

Flows through curved tubes have been studied by many investigators for several applications, particularly in vascular fluid dynamics. Most of the arteries are moderately curved and blood flow through them is affected by centrifugal forces which tend to set up secondary motions, recirculating fluid vortices and cause a non-symmetric distribution of the pressure and of the wall shear stress. The nature of these secondary flows have been examined in many papers in the past and an extensive list of references is provided below. However, little attention has been given to address the effect of the curvature on all the components of the flow velocity and on the pressure.

In Doppler measurements, all the velocity components are expected to contribute to the ultrasound signal: though the non-axial components do not alter the overall flow rate, their presence may cause a over/under estimation of the Doppler measurements and may change the waveforms used for clinical diagnosis of various pathological conditions. Thus it is worth quantifying the expected degree of variation of the Doppler waveform with corresponding variations in the curvature. Another relevant aspect of the curvature is the influence on wall shear stresses in relation to atherosclerotic diseases and the examination of time varying flow rates.

* Corresponding author.
E-mail addresses: pontrelli@iac.rm.cnr.it (G. Pontrelli), tatone@ing.univaq.it (A. Tatone).

0997-7546/$ – see front matter
doi:10.1016/j.euromechflu.2005.12.001

The earliest theoretical studies were conducted by Dean [1,2], who analyzed the steady laminar flow in a rigid curved pipe by a perturbation method. His study was limited to small values of the Dean number, $D_n = (a/R)^{1/2}Re$, where a is the radius of the pipe cross section, R the radius of curvature of the pipe axis and Re is the Reynolds number. Many further theoretical, numerical and experimental studies on this work have been conducted and have extended the range of the solution to larger Dean numbers, [3,4].

The problem of unsteady flow is more complicated and the simplification to a pure oscillatory flow has been considered in many studies. This work was initiated by Lyne [5] who used boundary-layer approximations to solve linearized Navier–Stokes equations for large values of the frequency parameter $\alpha = a(\omega/\nu)^{1/2}$. His results showed the existence of a four-vortex secondary flow system which could be divided into two regions: a core region in which the flow is essentially inviscid and a boundary region in which viscous effects dominate. The net effect was the shifting of the maximum axial velocity towards the inner wall of the curvature. Lyne's studies were again confined to a rigid walled tube.

Zalosh and Nelson [6] carried out an analysis using finite Hankel integral transforms and a perturbation solution to linearize the Navier–Stokes equations and confirmed Lyne's results. Mullin and Greated [7] carried out a similar analysis using an analogous solution procedure. Difficulties in these methods were encountered at high frequencies, due to the lack of convergence of the inverse Hankel transform.

The oscillatory flow with a nonzero mean was investigated by Smith [8] who again used boundary-layer approximations to derive several different flow attributes ranging between the limiting cases of steady flow in curved tubes to purely oscillatory flow in straight pipes and later by Wang and Tarbell in a more applied context [9]. Extensive surveys of the previous works with some critical considerations are given in [10] and [11]. Further numerical investigations can be found in a couple of subsequent works by Hamakiotes and Berger [12] and [13]. Their results are obtained with the projection method, apply to tubes of arbitrary curvature and show the importance of frequency parameter in oscillatory flows, but once again they were relative to a rigid wall.

On the other hand, when considering physiological applications, wall compliance and its interaction with the fluid constitute essential aspects that cannot be disregarded [14,15]. A mathematical analysis of pulsatile flow in a curved distensible tube was done by Chandran et al. in Refs. [16,17], where a thin-walled model was used in conjunction with the linearized Navier–Stokes equations and a numerical solution was given. A subsequent numerical study evidenced some other aspects of the fluid flow, and focused on the axial velocity flow waveforms and flow rate correction, but other important issues such as secondary flow and wall shear stress analysis were missing [18].

Based on the previous works, the purpose of this study is to present a unifying consistent and self-contained theory for such a problem. We extend the works in [16] and [18] by presenting the theory in a more general framework and deriving the governing equations through a number of simplifying assumptions. All limiting cases are included, and it is shown how previous theories can be recovered as special cases. In Section 2 the general 3D mechanics formulation for the fluid–structure problem is presented in its simplest basic form (Newtonian fluid, linear elasticity, thin wall). Next, the equations are linearized and expressed in a convenient coordinate system suitable to evidence the role of curvature (Section 3). Being interested in a propagative phenomenon, a wave solution superimposed onto a steady basic flow is considered (Section 4). This corresponds to apply a Fourier analysis and to split the solution into a steady and an unsteady components which are separately considered. The equations for the unsteady flow are derived through a scaling based on the characteristic of the pressure wave in typical physiological flows. A perturbation analysis over the curvature parameter a/R is presented in Section 5: though limited to small values of curvature, this approach has the advantage to recast the flow in a curved tube as a small correction due to the curvature over the flow in a straight elastic pipe. The 0th order solution is the classical Womersley solution [19]. The first order problem is reduced to a system of ordinary differential equations and a finite difference method is used to find approximate solutions (Section 6). Finally, in Section 7 several numerical results are presented: the effects of curvature on the secondary flow, on the pressure distribution and on the velocity patterns are shown.

2. Formulation of the problem

The motion of the blood in a curved vessel is modelled by the flow of a viscous Newtonian fluid through a curved elastic tube. The fluid flow, by virtue of the contact force, induces a wall deformation and, in turn, the wall deformation

modifies the fluid domain (*fluid–structure interaction*). To model the vessel wall, we assume that its thickness is small and use the theory of elastic membranes. Let us consider the fluid (blood) balance law

$$\operatorname{div} \boldsymbol{T} - \rho \boldsymbol{a} = 0, \tag{2.1}$$

and the solid (arterial wall) balance law

$$\operatorname{div}_s \boldsymbol{S} - \rho_w \boldsymbol{a}_w - \boldsymbol{T}\boldsymbol{n} + \boldsymbol{b} = 0, \tag{2.2}$$

with ρ, ρ_w the fluid and the wall densities, $\boldsymbol{a}$, $\boldsymbol{a}_w$ the fluid and the wall material accelerations, and $\boldsymbol{n}$ the external unit normal to the wall. In the above equations $\boldsymbol{T}$ and $\boldsymbol{S}$ are the fluid and the wall stress tensors. The surface force $\boldsymbol{b}$ describes any kind of interaction of the vascular wall with the surrounding tissues.

In a linear fluid, the response function for the fluid stress tensor is [20]

$$\boldsymbol{T} = -p\boldsymbol{I} + 2\mu \boldsymbol{D}, \tag{2.3}$$

where p is the pressure, μ the viscosity, and

$$\boldsymbol{D} := \operatorname{sym} \nabla \boldsymbol{v} = \frac{1}{2}\big(\nabla \boldsymbol{v} + (\nabla \boldsymbol{v})^{\mathrm{T}}\big).$$

The expression for the acceleration term in (2.1) is

$$\boldsymbol{a} = \frac{\partial \boldsymbol{v}}{\partial t} + (\nabla \boldsymbol{v})\boldsymbol{v}. \tag{2.4}$$

The fluid incompressibility condition reads as

$$\operatorname{div} \boldsymbol{v} = 0. \tag{2.5}$$

By substituting the above expressions into the balance law equation (2.1) we get the Navier–Stokes equation [21]

$$\rho\left[\frac{\partial \boldsymbol{v}}{\partial t} + (\nabla \boldsymbol{v})\,\boldsymbol{v}\right] = -\nabla p + \mu \Delta \boldsymbol{v}. \tag{2.6}$$

The variables p and $\boldsymbol{v}$ entering the above equations are fields on the fluid domain $\mathcal{D}$ which, because of the wall deformability, changes in time [22]. The evolution of the moving domain is described by a *grid deformation* function

$$\boldsymbol{\gamma} : \overline{\mathcal{D}} \times \mathbb{R} \to \mathcal{D}(t)$$

transforming a fixed domain $\overline{\mathcal{D}}$ into the current domain $\mathcal{D}$, at any time t. In $\overline{\mathcal{D}}$ we have:

$$\mathbf{v}(\bar{\boldsymbol{x}}, t) = \boldsymbol{v}\big(\boldsymbol{\gamma}(\bar{\boldsymbol{x}}, t), t\big)$$

and, after some computations, the new form of the Navier–Stokes equation in the undeformed domain $\overline{\mathcal{D}}$ becomes

$$\rho\left[\frac{\partial \mathbf{v}}{\partial t} + \nabla \mathbf{v}\boldsymbol{\Gamma}^{-1}\left(\mathbf{v} - \frac{\partial \boldsymbol{\gamma}}{\partial t}\right)\right] \det \boldsymbol{\Gamma} = -\boldsymbol{\Gamma}^{\star} \nabla p + 2\mu \operatorname{div}\big[\operatorname{sym}\big(\nabla \mathbf{v}\boldsymbol{\Gamma}^{-1}\big)\boldsymbol{\Gamma}^{\star}\big] \tag{2.7}$$

where

$$\boldsymbol{\Gamma} := \nabla \boldsymbol{\gamma}, \qquad \boldsymbol{\Gamma}^{\star} := (\det \boldsymbol{\Gamma})\boldsymbol{\Gamma}^{-\mathsf{T}}.$$

Similarly, the incompressibility condition (2.5) in $\overline{\mathcal{D}}$ is

$$\operatorname{div} \boldsymbol{v} = \operatorname{tr}\big(\nabla \mathrm{v}\boldsymbol{\Gamma}^{-1}\big) = \nabla \mathbf{v}^{\mathsf{T}} \cdot \boldsymbol{\Gamma}^{-1} = 0 \tag{2.8}$$

Eq. (2.2) is also rewritten in the fixed domain $\overline{\mathcal{D}}$, leading to a balance law in terms of Piola–Kirchhoff stress

$$\operatorname{div}_s\big(\big\|\boldsymbol{\Gamma}^{\star}\bar{\boldsymbol{n}}\big\|\boldsymbol{\Gamma}^{-\mathsf{T}}\boldsymbol{S}\big) - \bar{\rho}_w \frac{\partial^2 \boldsymbol{u}}{\partial^2 t} - \boldsymbol{T}\boldsymbol{\Gamma}^{\star}\bar{\boldsymbol{n}} + \big\|\boldsymbol{\Gamma}^{\star}\bar{\boldsymbol{n}}\big\|\boldsymbol{b} = 0, \tag{2.9}$$

where $\boldsymbol{u}$ is the wall displacement, $\bar{\rho}_w$ is the mass density of the fixed wall, $\bar{\boldsymbol{n}}$ is the external unit normal to $\partial\overline{\mathcal{D}}$.

The matching between the wall deformation and the grid deformation on $\partial\overline{\mathcal{D}}$ is enforced by

$$\boldsymbol{\gamma}(\bar{\boldsymbol{x}}, t) = \bar{\boldsymbol{x}} + \boldsymbol{u}(\bar{\boldsymbol{x}}, t).$$

The no slip condition on the fluid–wall interface is:

$$\mathbf{v} = \frac{\partial \boldsymbol{u}}{\partial t}. \tag{2.10}$$

3. Linearization and geometry

It is well known that the vascular flow can be decomposed into a steady dominant part and an oscillatory component over it [23]. As a consequence, it is reasonable to look for a solution made up of an *unsteady* component superimposed to a steady (or *base*) solution. Let us assume the unsteady solution be *small* enough that it can be linearized over the steady state solution[1]

$$\chi = \bar{\chi} + \delta\hat{\chi}, \tag{3.1}$$

with δ a scaling parameter of the unsteady component.

We assume that $\overline{\mathcal{D}}$ is the domain corresponding to the steady solution. Hence the grid deformation function and its gradient can be linearized as

$$\boldsymbol{\gamma} = \bar{\boldsymbol{\gamma}} + \delta\hat{\boldsymbol{\gamma}}, \qquad \boldsymbol{\Gamma} = \overline{\boldsymbol{\Gamma}} + \delta\widehat{\boldsymbol{\Gamma}},$$

where $\bar{\boldsymbol{\gamma}}$ is the identity map and, as a consequence, $\overline{\boldsymbol{\Gamma}} = \boldsymbol{I}$. The linearization of Eqs. (2.7) and (2.9) leads to two different equations for the steady and for the unsteady flows. The latter contains terms with $\hat{\boldsymbol{\gamma}}$ and $\widehat{\boldsymbol{\Gamma}}$ due to the nonzero steady solution that cannot *a priori* be omitted. This was not pointed out in other previous works, for which some aspects of the linearization procedure is deemed questionable [16,17]. The importance of such terms depends on the Young modulus E (see below): the higher it is, the stiffer the wall and minor the role of $\hat{\boldsymbol{\gamma}}$ and $\widehat{\boldsymbol{\Gamma}}$. In other words, a low wall compliance can justify neglecting the grid deformation terms in Eqs. (2.7), (2.8) and (2.9). This allows us to consider all variables in Eqs. (2.1), (2.2) and (2.10) as fields on the undeformed domain $\overline{\mathcal{D}}$. Some preliminary results evidenced a minor role of such terms and allow us to cancel them out. A thorough study of the fluid–structure interaction problem in the general case, will be carried out in a future investigation.

The surface force $\boldsymbol{b}$ in Eq. (2.2) is also linearized as:

$$\boldsymbol{b} = \bar{\boldsymbol{b}} + \delta\hat{\boldsymbol{b}}.$$

A reasonable assumption is that $\bar{\boldsymbol{b}}$ balances the surface force exerted by the fluid on the wall, letting the corresponding stress to be zero. On the other hand, the term $\hat{\boldsymbol{b}}$ describes a wall constrained force known as *tethering* [23]. In this work this effect is neglected, setting $\hat{\boldsymbol{b}} = 0$.

Once the linearization over the steady flow has been carried out, the value of the parameter δ is set equal to one.

Let us now consider the case where $\overline{\mathcal{D}}$ is a portion of torus having a planar axis, a circular cross section of radius a and a radius of curvature R (Fig. 1(a)). With such a geometry, it is convenient to parametrize the domain with a toroidal coordinate system (r, ψ, θ) (see Fig. 1(b)) and to use components in the corresponding orthonormal basis. Let us denote by (u, v, w) the radial, circumferential and axial components of the fluid velocity $\boldsymbol{v}$, and by (η, ξ, ζ) the corresponding components of the wall displacement $\boldsymbol{u}$. In the appendix the scalar form of the differential equations corresponding to Eqs. (2.5), (2.6), (2.2), (2.10) before linearization is given. The axial variable $z = R\theta$ is introduced to avoid degeneracy when $R \to \infty$, and all the variables are rewritten as functions of z instead of θ, in all the governing equations.

In Eq. (2.2), a linearly elastic isotropic material for the wall is adopted. Indicating by $(\epsilon_{zz}, \epsilon_{z\psi}, \epsilon_{\psi\psi})$ the components of the strain tensor, the membrane stress matrix is given by

$$\begin{pmatrix} S_{zz} & S_{z\psi} \\ S_{\psi z} & S_{\psi\psi} \end{pmatrix} = \begin{pmatrix} hB(\epsilon_{zz} + \sigma\epsilon_{\psi\psi}) & 2hG\epsilon_{z\psi} \\ 2hG\epsilon_{z\psi} & hB(\epsilon_{\psi\psi} + \sigma\epsilon_{zz}) \end{pmatrix} \tag{3.2}$$

with

$$B := \frac{E}{1-\sigma^2}, \qquad G := \frac{E}{2(1+\sigma)}$$

being E the Young modulus, σ the Poisson ratio and h the wall thickness.

[1] From now on, we shortly indicate by χ the global solution of the fluid–structure interaction problem.

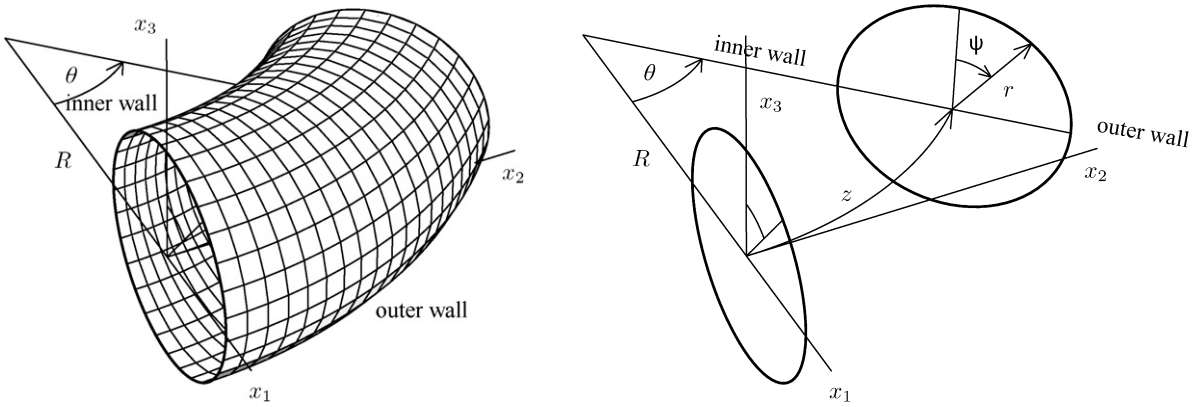

Fig. 1. A portion of the curved tube between two cross sections (a). Toroidal coordinates (r, ψ, θ) and Cartesian coordinates (x_1, x_2, x_3) (b).

4. Wave solution

We now assume that, in the linearized solution (3.1), the unsteady part has the form of a fully developed travelling wave:

$$\begin{aligned}
&\bar{u}(r,\psi) + \hat{u}(r,\psi,z,t) = \bar{u}(r,\psi) + \tilde{u}(r,\psi)\,\mathrm{e}^{\mathrm{i}(\omega t - kz)},\\
&\bar{v}(r,\psi) + \hat{v}(r,\psi,z,t) = \bar{v}(r,\psi) + \tilde{v}(r,\psi)\,\mathrm{e}^{\mathrm{i}(\omega t - kz)},\\
&\overline{w}(r,\psi) + \widehat{w}(r,\psi,z,t) = \overline{w}(r,\psi) + \widetilde{w}(r,\psi)\,\mathrm{e}^{\mathrm{i}(\omega t - kz)},\\
&\bar{p}(r,\psi) + \hat{p}(r,\psi,z,t) = \bar{p}(r,\psi,z) + \tilde{p}(r,\psi)\,\mathrm{e}^{\mathrm{i}(\omega t - kz)},\\
&\bar{\eta}(\psi) + \hat{\eta}(\psi,z,t) = \bar{\eta}(\psi) + \tilde{\eta}(\psi)\,\mathrm{e}^{\mathrm{i}(\omega t - kz)},\\
&\bar{\xi}(\psi) + \hat{\xi}(\psi,z,t) = \bar{\xi}(\psi) + \tilde{\xi}(\psi)\,\mathrm{e}^{\mathrm{i}(\omega t - kz)},\\
&\bar{\zeta}(\psi) + \hat{\zeta}(\psi,z,t) = \bar{\zeta}(\psi) + \tilde{\zeta}(\psi)\,\mathrm{e}^{\mathrm{i}(\omega t - kz)}
\end{aligned} \tag{4.1}$$

where ω is the circular frequency, k the wave number and $c = \omega/k$ the complex wave speed.

After linearization, a further step consists in a scaling procedure concerning the relative magnitudes of some terms, by means of some hypothesis on the wave characteristics. It is well known that in blood flow propagation phenomena, the wavelength $\lambda = 1/k = c/\omega$ is large compared with the vessel's radius a [23]. On the other hand, the flow being essentially unidirectional, the longitudinal velocity w is much larger than the other two velocity components. This is expressed by the following scaling:

$$\frac{\tilde{u}}{\widetilde{w}} \approx \frac{\tilde{v}}{\widetilde{w}} \approx \widetilde{w} = \mathrm{O}\left(\frac{a}{\lambda}\right)$$

and leads to a simplification of the unsteady flow equations: only the terms of the lowest order in a/λ in each equation are retained and those of higher order are neglected.

Concerning the steady solution, this has been analyzed by Dean who found an analytical solution for a steady flow in a curved rigid walled tube [1,2]. He used a perturbation approach based on the curvature parameter $\varepsilon = a/R$, which is supposed to be small, such that the solution up to the first order is $\bar{\chi} = \bar{\chi}_0 + \varepsilon\bar{\chi}_1$, being $\bar{\chi}_0$ the steady state solution in a straight rigid tube (Hagen–Poiseuille flow [21]), and $\bar{\chi}_1$ is the correction due to the curvature. One has:

$$\bar{p}_0 = -4\mu H z; \qquad \bar{u}_0 = \bar{v}_0 = 0; \qquad \overline{w}_0(r) = H\left(a^2 - r^2\right) = \frac{(\mathrm{d}\bar{p}_0/\mathrm{d}z)(a^2 - r^2)}{4\mu}, \tag{4.2}$$

Then, by assuming:

$$\begin{aligned}
&\bar{p}_1(r,\psi) = \check{p}_1(r)\sin\psi,\\
&\bar{u}_1(r,\psi) = \check{u}_1(r)\sin\psi,\\
&\bar{v}_1(r,\psi) = \check{v}_1(r)\cos\psi,\\
&\overline{w}_1(r,\psi) = \check{w}_1(r)\sin\psi
\end{aligned} \tag{4.3}$$

an exact solution of the first order problem is given in the form [1]:

$$\begin{aligned}
\check{p}_1(r) &= \frac{\rho H^2 r(2r^4 - 6r^2a^2 + 9a^4)}{12a},\\
\check{u}_1(r) &= \frac{H^2(a^2-r^2)^2(4a^2-r^2)}{288a\nu},\\
\check{v}_1(r) &= \frac{H^2(a^2-r^2)(7r^4 - 23a^2r^2 + 4a^4)}{288a\nu},\\
\check{w}_1(r) &= -\frac{3Hr(a^2-r^2)}{4a} + \frac{H^3 r}{1152a\nu^2}\left[4a^6\left(a^2-r^2\right) - 3a^4\left(a^4-r^4\right) + a^2\left(a^6-r^6\right) - \frac{a^8-r^8}{10}\right]
\end{aligned} \tag{4.4}$$

with $\nu = \mu/\rho$ the kinematic viscosity. In the following, such procedure will be extended to the unsteady flow in a curved tube with elastic walls.

Finally, the unsteady part of the flow equations (A1)–(A4), after linearization and scaling, become:

Incompressibility equation:

$$\frac{\partial\hat{u}}{\partial r} + \frac{\hat{u}}{r} + \frac{1}{r}\frac{\partial\hat{v}}{\partial\psi} + \frac{\hat{u}\sin\psi}{R + r\sin\psi} + \frac{\hat{v}\cos\psi}{R + r\sin\psi} + \frac{R}{R + r\sin\psi}\frac{\partial\widehat{w}}{\partial z} = 0. \tag{4.5}$$

Flow equations:

$$\begin{aligned}
\rho\left(\frac{\partial\hat{u}}{\partial t} - \frac{2\overline{w}\widehat{w}\sin\psi}{R + r\sin\psi}\right) = &-\frac{\partial\hat{p}}{\partial r} + \mu\left(\frac{\partial^2\hat{u}}{\partial r^2} + \frac{1}{r}\frac{\partial\hat{u}}{\partial r} + \frac{1}{r^2}\frac{\partial^2\hat{u}}{\partial\psi^2} + \frac{\sin\psi}{R + r\sin\psi}\frac{\partial\hat{u}}{\partial r} + \frac{\cos\psi}{r(R + r\sin\psi)}\frac{\partial\hat{u}}{\partial\psi} - \frac{\hat{u}}{r^2}\right.\\
&- \frac{2}{r^2}\frac{\partial\hat{v}}{\partial\psi} - \frac{\hat{v}R\cos\psi}{r(R + r\sin\psi)^2} - \frac{2R\sin\psi}{(R + r\sin\psi)^2}\frac{\partial\widehat{w}}{\partial z}\\
&\left.- \frac{\hat{u}\sin^2\psi}{(R + r\sin\psi)^2} - \frac{2\hat{v}\sin\psi\cos\psi}{(R + r\sin\psi)^2}\right),
\end{aligned} \tag{4.6}$$

$$\begin{aligned}
\rho\left(\frac{\partial\hat{v}}{\partial t} - \frac{2\overline{w}\widehat{w}\cos\psi}{R + r\sin\psi}\right) = &-\frac{1}{r}\frac{\partial\hat{p}}{\partial\psi} + \mu\left(\frac{\partial^2\hat{v}}{\partial r^2} + \frac{1}{r}\frac{\partial\hat{v}}{\partial r} + \frac{1}{r^2}\frac{\partial^2\hat{v}}{\partial\psi^2} + \frac{2}{r^2}\frac{\partial\hat{u}}{\partial\psi}\right.\\
&+ \frac{\hat{u}R\cos\psi}{r(R + r\sin\psi)^2} + \frac{\sin\psi}{R + r\sin\psi}\frac{\partial\hat{v}}{\partial r} + \frac{\cos\psi}{r(R + r\sin\psi)}\frac{\partial\hat{v}}{\partial\psi} - \frac{\hat{v}}{r^2}\\
&\left.- \frac{2R\cos\psi}{(R + r\sin\psi)^2}\frac{\partial\widehat{w}}{\partial z} - \frac{\hat{v}\cos^2\psi}{(R + r\sin\psi)^2}\right),
\end{aligned} \tag{4.7}$$

$$\begin{aligned}
\rho\frac{\partial\widehat{w}}{\partial t} = &-\frac{R}{R + r\sin\psi}\frac{\partial\hat{p}}{\partial z} + \mu\left(\frac{\partial^2\widehat{w}}{\partial r^2} + \frac{1}{r}\frac{\partial\widehat{w}}{\partial r} + \frac{1}{r^2}\frac{\partial^2\widehat{w}}{\partial\psi^2} + \frac{\sin\psi}{R + r\sin\psi}\frac{\partial\widehat{w}}{\partial r}\right.\\
&\left.+ \frac{\cos\psi}{r(R + r\sin\psi)}\frac{\partial\widehat{w}}{\partial\psi} - \frac{\widehat{w}}{(R + r\sin\psi)^2}\right).
\end{aligned} \tag{4.8}$$

Let us note that the axial velocity equation is decoupled from the other motion equations except for the pressure term in Eq. (4.8) which relates it to the transverse components. Differently from the procedure in [16], the linearization of the convection term ($\overline{w}\widehat{w}$ in l.h.s. of Eqs. (4.6), (4.7)) enforces a strong coupling with the base flow. It turns out that the secondary flow is triggered by the base axial velocity $\overline{w} \neq 0$.

The wall motion equations and the fluid–wall interface conditions (Eqs. (A.5)–(A.8)) are rewritten in terms of the coordinate z and listed here for completeness.

Wall equations:

$$\rho_w h\frac{\partial^2\hat{\eta}}{\partial t^2} = \left[\hat{p} - 2\mu\frac{\partial\hat{u}}{\partial r}\right]_{r=a} - hB\left[\frac{\hat{\eta} + \partial\hat{\xi}/\partial\psi}{a^2} + \frac{\sin\psi(\hat{\eta}\sin\psi + \hat{\xi}\cos\psi + R\partial\hat{\zeta}/\partial z)}{(R + a\sin\psi)^2}\right] - \sigma hB\left[\frac{\sin\psi(2\hat{\eta} + \partial\hat{\xi}/\partial\psi) + \hat{\xi}\cos\psi + R\partial\hat{\zeta}/\partial z}{a(R + a\sin\psi)}\right], \tag{4.9}$$

$$\rho_w h\frac{\partial^2\hat{\xi}}{\partial t^2} = -\mu\left[\frac{1}{a}\frac{\partial\hat{u}}{\partial\psi} - \frac{\hat{v}}{a} + \frac{\partial\hat{v}}{\partial r}\right]_{r=a} + hB\left[\frac{\partial\hat{\eta}/\partial\psi + \partial^2\hat{\xi}/\partial\psi^2}{a^2} + \cos\psi\left(\frac{\hat{\eta} + \partial\hat{\xi}/\partial\psi}{a(R + a\sin\psi)} - \frac{\hat{\eta}\sin\psi + \hat{\xi}\cos\psi + R\partial\hat{\zeta}/\partial z}{(R + a\sin\psi)^2}\right)\right] + \sigma hB\left[\frac{-\hat{\xi}\sin\psi + \sin\psi\,\partial\hat{\eta}/\partial\psi + R\partial^2\hat{\zeta}/\partial\psi\partial z}{a(R + a\sin\psi)}\right] + hG\left[\frac{R\hat{\partial}^2\zeta/\partial z\partial\psi}{a(R + a\sin\psi)} + \frac{R^2\partial^2\hat{\xi}/\partial z^2 - R\cos\psi\,\partial\hat{\zeta}/\partial z}{(R + a\sin\psi)^2}\right]. \tag{4.10}$$

$$\rho_w h\frac{\partial^2\hat{\zeta}}{\partial t^2} = -\mu\left[\frac{R}{R + a\sin\psi}\frac{\partial\hat{u}}{\partial z} - \frac{\widehat{w}\sin\psi}{R + a\sin\psi} + \frac{\partial\hat{w}}{\partial r}\right]_{r=a} + hB\left[\frac{R\sin\psi\,\partial\hat{\eta}/\partial z + R\cos\psi\,\partial\hat{\xi}/\partial z + R^2\partial^2\hat{\zeta}/\partial z^2}{(R + a\sin\psi)^2}\right] + \sigma hB\left[\frac{R\partial\hat{\eta}/\partial z + R\partial^2\hat{\xi}/\partial\psi\partial z}{a(R + a\sin\psi)}\right] + hG\left[\frac{1}{a^2}\frac{\partial^2\hat{\zeta}}{\partial\psi^2} + \frac{R\partial^2\hat{\xi}/\partial\psi\partial z + \hat{\zeta}\sin\psi + \cos\psi\,\partial\hat{\zeta}/\partial\psi}{a(R + a\sin\psi)} + \frac{R\cos\psi\,\partial\hat{\xi}/\partial z - \hat{\zeta}\cos^2\psi}{(R + a\sin\psi)^2}\right]. \tag{4.11}$$

Interface conditions:

$$\frac{\partial\hat{\eta}}{\partial t} = \hat{u}|_{r=a}, \quad \frac{\partial\hat{\xi}}{\partial t} = \hat{v}|_{r=a}, \quad \frac{\partial\hat{\zeta}}{\partial t} = \widehat{w}|_{r=a}, \tag{4.12}$$

5. Perturbation solution

A perturbation method is used to study the influence of the curvature with respect to the straight case. First of all, Eqs. (4.5)–(4.8) are rewritten in terms of a normalized radial variable $y = r/a$ ($0 \leqslant y \leqslant 1$).

As the curvature parameter $\varepsilon = a/R$ is assumed to be small ($\ll 1$), the tilded quantities (amplitudes) in Eqs. (4.1) are expanded as a power series of ε over an axisymmetric solution $\chi_0(y)$. We have:

$$\begin{aligned}
\tilde{p}(y,\psi) &= p_0(y) + \varepsilon p_1(y,\psi) + \varepsilon^2 p_2(y,\psi) + \cdots,\\
\tilde{u}(y,\psi) &= u_0(y) + \varepsilon u_1(y,\psi) + \varepsilon^2 u_2(y,\psi) + \cdots,\\
\tilde{v}(y,\psi) &= v_0(y) + \varepsilon v_1(y,\psi) + \varepsilon^2 v_2(y,\psi) + \cdots,\\
\widetilde{w}(y,\psi) &= w_0(y) + \varepsilon w_1(y,\psi) + \varepsilon^2 w_2(y,\psi) + \cdots,\\
\tilde{\eta}(\psi) &= \eta_0 + \varepsilon\eta_1(\psi) + \varepsilon^2\eta_2(\psi) + \cdots,\\
\tilde{\xi}(\psi) &= \xi_0 + \varepsilon\xi_1(\psi) + \varepsilon^2\xi_2(\psi) + \cdots,\\
\tilde{\zeta}(\psi) &= \zeta_0 + \varepsilon\zeta_1(\psi) + \varepsilon^2\zeta_2(\psi) + \cdots
\end{aligned} \tag{5.1}$$

similarly to the procedure described in Section 4 for the steady solution $\bar{\chi}$. These expansions are substituted in Eqs. (4.5)–(4.12), and terms of the same power of ε, up to the first order, are equated.

5.1. Zero-th order solution

In the asymptotic expansion equation (5.1), χ_0 corresponds to the axisymmetric solution in a straight tube. The procedure to compute it is shortly reminded here. The interested reader is referred to the Womersley paper for a full description and for further mathematical details [19]. Being $v_0 = 0$, $\xi_0 = 0$, $\partial/\partial\psi = 0$, we have:

Incompressibility equation:

$$\frac{\mathrm{d}u_0}{\mathrm{d}y} + \frac{u_0}{y} - \mathrm{i}ka w_0 = 0. \tag{5.2}$$

Flow equations:

$$\frac{\mathrm{d}^2u_0}{\mathrm{d}y^2} + \frac{1}{y}\frac{\mathrm{d}u_0}{\mathrm{d}y} - \frac{u_0}{y^2} - \mathrm{i}\alpha^2 u_0 = \frac{a}{\mu}\frac{\mathrm{d}p_0}{\mathrm{d}y}, \tag{5.3}$$

$$\frac{\mathrm{d}^2w_0}{\mathrm{d}y^2} + \frac{1}{y}\frac{\mathrm{d}w_0}{\mathrm{d}y} - \mathrm{i}\alpha^2 w_0 = -\frac{\mathrm{i}ka^2}{\mu}p_0. \tag{5.4}$$

Wall equations:

$$-\omega^2\eta_0 = \frac{B}{\rho_w}\left(\mathrm{i}k\sigma\frac{\zeta_0}{a} - \frac{\eta_0}{a^2}\right) + \frac{1}{\rho_w h}[p_0]_{y=1}, \tag{5.5}$$

$$-\omega^2\zeta_0 = -\frac{B}{\rho_w}\left(k^2\zeta_0 + \mathrm{i}k\sigma\frac{\eta_0}{a}\right) - \frac{1}{\rho_w h}\frac{\mu}{a}\left[\frac{\mathrm{d}w_0}{\mathrm{d}y}\right]_{y=1} \tag{5.6}$$

where the terms u_0 and $\mathrm{d}u_0/\mathrm{d}y$ at the wall are small and have been neglected, $\alpha = a\sqrt{\omega/\nu}$ (Womerseley number).

Interface conditions:

$$\mathrm{i}\omega\eta_0 = u_0|_{y=1}, \qquad \mathrm{i}\omega\zeta_0 = w_0|_{y=1}. \tag{5.7}$$

Eqs. (5.2)–(5.6) form an eigenvalue problem and provide a couple (ω, k) which corresponds to an admissible solution. We now assume that:

$$p_0(y) = AJ_0(\beta y)$$

with A a constant and β is to be determined. By using a number of approximations due to the relative order of magnitude (i.e. $k^2a^2 \ll \alpha^2$), we obtain that $\beta = \mathrm{i}ka$ and:

$$p_0(y) \approx AI_0(\beta y) \approx A. \tag{5.8}$$

Then, we can easily integrate the fluid equations (5.3) and (5.4) obtaining [19]:

$$u_0(y) = \frac{\mathrm{i}ka}{2}\left[C\frac{2J_1(\alpha\mathrm{i}^{3/2}y)}{\alpha i^{3/2}J_0(\alpha\mathrm{i}^{3/2})} + \frac{Aky}{\rho\omega}\right], \tag{5.9}$$

$$w_0(y) = C\frac{J_0(\alpha\mathrm{i}^{3/2}y)}{J_0(\alpha\mathrm{i}^{3/2})} + \frac{Ak}{\rho\omega} \tag{5.10}$$

where J_0 and J_1 denote the first kind and 0th and 1th order Bessel functions respectively. Pressure and fluid velocities (5.8)–(5.10), evaluated on the wall, are finally substituted in Eqs. (5.5), (5.6) and in the matching conditions (5.7). The set of the four algebraic equations (5.5)–(5.7) constitute a homogeneous algebraic system in the four unknowns A, C, η_0, ζ_0. The determinant of such system equated to zero leads, after some algebraic manipulations, to the following so called *frequency equation*:

$$4(1-F_{10})\left(\frac{c_0}{c}\right)^4 - 2\left[2+\gamma(1-F_{10}) + F_{10}\left(\frac{1}{2}-2\sigma\right)\right]\left(\frac{c_0}{c}\right)^2 + (F_{10}+2\gamma)\left(1-\sigma^2\right) = 0 \tag{5.11}$$

where

$$F_{10}(\alpha) = \frac{2J_1(\alpha\mathrm{i}^{3/2})}{\alpha i^{3/2}J_0(\alpha\mathrm{i}^{3/2})}, \qquad \gamma = \frac{h\rho_w}{a\rho}, \qquad c_0^2 = \frac{Eh}{2a\rho}.$$

Eq. (5.11) admits two values for k^2 as solution and, because of the large wavelength of pressure waves, the smaller one is chosen. The ∞^2 dimensional space of solutions $(p_0, u_0, w_0, \eta_0, \zeta_0)$ is then determined in correspondence of $\pm k$.

It is worth noting that for a rigid wall tube ($E \to \infty$), $k \to 0$ and $c \to \infty$. Such a case is inconsistent with the wave propagation assumption equations (4.1) and has not been considered here (see Section 7.1 for a discussion).

6. First order solution

By equating the 1st order terms in the governing fluid–structure equations (4.5)–(4.12), we get the first order equations for a moderately curved tube:

Incompressibility equation:

$$\frac{\partial u_1}{\partial y}+\frac{u_1}{y}+\frac{1}{y}\frac{\partial v_1}{\partial \psi}-\mathrm{i}kaw_1=(-\mathrm{i}kayw_0-u_0)\sin\psi. \tag{6.1}$$

Flow equations:

$$\frac{\partial^2 u_1}{\partial y^2}-\frac{u_1}{y^2}+\frac{1}{y}\frac{\partial u_1}{\partial y}+\frac{1}{y^2}\frac{\partial^2 u_1}{\partial \psi^2}-\frac{2}{y^2}\frac{\partial v_1}{\partial \psi}-\mathrm{i}\alpha^2 u_1-\frac{a}{\mu}\frac{\partial p_1}{\partial y}=-\left(\frac{du_0}{dy}+2\mathrm{i}kaw_0+2\frac{a\overline{w}_0}{\nu}w_0\right)\sin\psi, \tag{6.2}$$

$$\frac{\partial^2 v_1}{\partial y^2}-\frac{v_1}{y^2}+\frac{1}{y}\frac{\partial v_1}{\partial y}+\frac{1}{y^2}\frac{\partial^2 v_1}{\partial \psi^2}+\frac{2}{y^2}\frac{\partial u_1}{\partial \psi}-\mathrm{i}\alpha^2 v_1-\frac{a}{\mu y}\frac{\partial p_1}{\partial \psi}=-\left(\frac{u_0}{y}+2\mathrm{i}kaw_0+2\frac{a\overline{w}_0}{\nu}w_0\right)\cos\psi, \tag{6.3}$$

$$\frac{\partial^2 w_1}{\partial y^2}+\frac{1}{y}\frac{\partial w_1}{\partial y}+\frac{1}{y^2}\frac{\partial^2 w_1}{\partial \psi^2}-\mathrm{i}\alpha^2 w_1+\frac{\mathrm{i}ka^2}{\mu}p_1=-\left(\frac{\mathrm{d}w_0}{\mathrm{d}y}-\frac{\mathrm{i}ka^2 y}{\mu}p_0\right)\sin\psi. \tag{6.4}$$

Wall equations:

$$\left(1-\frac{\rho_w a^2\omega^2}{B}\right)\eta_1+\frac{\partial \xi_1}{\partial \psi}-\mathrm{i}ka\sigma\zeta_1=\frac{a}{Bh}\left[ap_1-2\mu\frac{\partial u_1}{\partial y}\right]_{y=1}-\left[2\sigma\eta_0+\mathrm{i}ka(\sigma-1)\zeta_0\right]\sin\psi, \tag{6.5}$$

$$\begin{aligned}&\frac{\partial^2 \xi_1}{\partial \psi^2}+\frac{\partial \eta_1}{\partial \psi}-\left(\frac{k^2a^2G}{B}-\frac{\rho_w a^2\omega^2}{B}\right)\xi_1-\mathrm{i}ka\left(\frac{G}{B}+\sigma\right)\frac{\partial \zeta_1}{\partial \psi}\\&\quad=\frac{a\mu}{Bh}\left[\frac{\partial u_1}{\partial \psi}+\frac{\partial v_1}{\partial y}-v_1\right]_{y=1}-\left[\eta_0+\mathrm{i}ka\left(1+\frac{G}{B}\right)\zeta_0\right]\cos\psi,\end{aligned} \tag{6.6}$$

$$\begin{aligned}&\left(\frac{\rho_w a^2\omega^2}{B}-k^2a^2\right)\zeta_1+\frac{G}{B}\frac{\partial^2 \zeta_1}{\partial \psi^2}-\mathrm{i}ka\sigma\eta_1-\mathrm{i}ka\left(\frac{G}{B}+\sigma\right)\frac{\partial \xi_1}{\partial \psi}\\&\quad=\frac{a\mu}{Bh}\left[\frac{\partial w_1}{\partial y}-\sin\psi\, w_0\right]_{y=1}-\left[\mathrm{i}ka(\sigma-1)\eta_0+\left(2k^2a^2+\frac{G}{B}\right)\zeta_0\right]\sin\psi.\end{aligned} \tag{6.7}$$

Interface conditions:

$$\mathrm{i}\omega\eta_1=u_1|_{y=1},\qquad \mathrm{i}\omega\xi_1=v_1|_{y=1},\qquad \mathrm{i}\omega\zeta_1=w_1|_{y=1}. \tag{6.8}$$

Note that the homogeneous part of the 1st order problem equals the 0th order equations (except for axisymmetry).

6.1. Separation of variables

Based on the form of r.h.s. of the previous Eqs. (6.1)–(6.8), we look for a solution of the form:

$$\begin{aligned}&p_1(y,\psi)=\breve{p}_1(y)\sin\psi,\\&u_1(y,\psi)=\breve{u}_1(y)\sin\psi,\\&v_1(y,\psi)=\breve{v}_1(y)\cos\psi,\\&w_1(y,\psi)=\breve{w}_1(y)\sin\psi,\\&\eta_1(\psi)=\breve{\eta}_1\sin\psi,\\&\xi_1(\psi)=\breve{\xi}_1\cos\psi,\\&\zeta_1(\psi)=\breve{\zeta}_1\sin\psi.\end{aligned} \tag{6.9}$$

By replacing such expressions in Eqs. (6.1)–(6.8) the problem reduces to a linear system of ordinary differential equations (by omitting the $\breve{}$ accent):

Incompressibility equation:

$$\frac{\mathrm{d}u_1}{\mathrm{d}y} + \frac{u_1}{y} - \frac{v_1}{y} - \mathrm{i}kaw_1 = -(\mathrm{i}kayw_0 + u_0). \tag{6.10}$$

Flow equations:

$$\frac{\mathrm{d}^2u_1}{\mathrm{d}y^2} + \frac{1}{y}\frac{\mathrm{d}u_1}{\mathrm{d}y} - \left(\frac{2}{y^2} + \mathrm{i}\alpha^2\right)u_1 + \frac{2v_1}{y^2} - \frac{a}{\mu}\frac{\mathrm{d}p_1}{\mathrm{d}y} = -\left(\frac{\mathrm{d}u_0}{\mathrm{d}y} + 2\mathrm{i}kaw_0 + 2\frac{a\overline{w}_0}{\nu}w_0\right), \tag{6.11}$$

$$\frac{\mathrm{d}^2v_1}{\mathrm{d}y^2} + \frac{1}{y}\frac{\mathrm{d}v_1}{\mathrm{d}y} - \left(\frac{2}{y^2} + \mathrm{i}\alpha^2\right)v_1 + \frac{2u_1}{y^2} - \frac{ap_1}{\mu y} = -\left(\frac{u_0}{y} + 2\mathrm{i}kaw_0 + 2\frac{a\overline{w}_0}{\nu}w_0\right), \tag{6.12}$$

$$\frac{\mathrm{d}^2w_1}{\mathrm{d}y^2} + \frac{1}{y}\frac{\mathrm{d}w_1}{\mathrm{d}y} - \left(\frac{1}{y^2} + \mathrm{i}\alpha^2\right)w_1 + \frac{\mathrm{i}ka^2}{\mu}p_1 = -\left(\frac{\mathrm{d}w_0}{\mathrm{d}y} - \frac{\mathrm{i}ka^2y}{\mu}p_0\right). \tag{6.13}$$

Wall equations:

$$\left(1 - \frac{\rho_w a^2\omega^2}{B}\right)\eta_1 - \xi_1 - \mathrm{i}ka\sigma\zeta_1 = \frac{a}{Bh}\left[ap_1 - 2\mu\frac{\mathrm{d}u_1}{\mathrm{d}y}\right]_{y=1} - 2\sigma\eta_0 + \mathrm{i}ka(1-\sigma)\zeta_0, \tag{6.14}$$

$$\begin{aligned}&-\left(1 + \frac{k^2a^2G}{B} - \frac{\rho_w a^2\omega^2}{B}\right)\xi_1 + \eta_1 - \mathrm{i}ka\left(\frac{G}{B} + \sigma\right)\zeta_1\\ &\quad = \frac{a\mu}{Bh}\left[u_1 + \frac{\mathrm{d}v_1}{\mathrm{d}y} - v_1\right]_{y=1} - \eta_0 - \mathrm{i}ka\left(1 + \frac{G}{B}\right)\zeta_0,\end{aligned} \tag{6.15}$$

$$\begin{aligned}&-\left(\frac{G}{B} + k^2a^2 - \frac{\rho_w a^2\omega^2}{B}\right)\zeta_1 - \mathrm{i}ka\sigma\eta_1 + \mathrm{i}ka\left(\frac{G}{B} + \sigma\right)\xi_1\\ &\quad = \frac{a\mu}{Bh}\left[\frac{\mathrm{d}w_1}{\mathrm{d}y} - w_0\right]_{y=1} - \mathrm{i}ka(\sigma-1)\eta_0 - \left(\frac{G}{B} + 2k^2a^2\right)\zeta_0.\end{aligned} \tag{6.16}$$

Interface conditions:

Because of the continuity of the physical variables in $y = 0$, the following boundary conditions are imposed at the origin:

$$u_1(0) = v_1(0), \qquad u_1'(0) = v_1'(0) = 0, \qquad p_1(0) = 0, \qquad w_1(0) = 0 \tag{6.17}$$

(see [1,2]) and the following fluid–wall matching velocity conditions are set at the wall (cf. Eqs. (6.8)):

$$\mathrm{i}\omega\eta_1 = u_1(1), \qquad \mathrm{i}\omega\xi_1 = v_1(1), \qquad \mathrm{i}\omega\zeta_1 = w_1(1). \tag{6.18}$$

The fluid–structure interaction first order problem is similar to the zero-th order problem, but lack of geometrical symmetry makes the search for analytical solutions hard. Therefore the nonhomogeneous system is solved numerically. The flow and the continuity equations (6.10)– (6.13) are discretized in [0, 1] by upwind finite differences [24]. Coupled with the flow equations, the wall motion equations (6.14)–(6.16) are solved together with the boundary conditions (6.17) in $y = 0$ and with the interface conditions (6.18) in $y = 1$. The value of k turns out to be very close to zero, which corresponds to a pure oscillating solution for a rigid wall (see Section 7.1). This is a cause of ill-conditioning of the first order problem whose numerical solution turns out to be dominated by a solution close to the *rigid one*. In order to get rid of this spurious solution, a procedure has been devised which, via a spectral decomposition, cancels out the projection onto the subspace of the least eigenvalue. This treatment turns out to be computationally very effective. An alternative way to overcome the ill-conditioning is to modify the original problem by adding the so-called tethering, as made in [25,16].

7. Computational results and discussion

Once the 0th order solution is obtained analytically and 1st order solution is computed numerically, the full solution is then reassembled as:

$$\chi = \bar{\chi} + \tilde{\chi}\,\mathrm{e}^{\mathrm{i}(\omega t - kz)} = (\bar{\chi}_0 + \varepsilon\bar{\chi}_1) + (\tilde{\chi}_0 + \varepsilon\tilde{\chi}_1)\,\mathrm{e}^{\mathrm{i}(\omega t - kz)}$$

(see Eq. (4.1)). An harmonic form of the previous expression is:

$$\chi = \bar{\chi} + \left[\mathrm{Re}(\tilde{\chi})\cos\left(\omega t - \mathrm{Re}(k)z\right) - \mathrm{Im}(\tilde{\chi})\sin\left(\omega t - \mathrm{Re}(k)z\right)\right] \mathrm{e}^{\mathrm{Im}(k)z} \tag{7.1}$$

or equivalently:

$$\chi = \bar{\chi} + |\tilde{\chi}|\cos\left(\omega t - \mathrm{Re}(k)z + \phi\right)\mathrm{e}^{\mathrm{Im}(k)z} \quad \text{with } \phi = \arg(\tilde{\chi}). \tag{7.2}$$

From Eq. (7.2), it follows that each variable has an oscillatory evolution in time, superimposed over the steady state solution, with amplitude $|\tilde{\chi}|$ and a phase lead or a phase lag ϕ. Both amplitude and phase are independent of time and depend on the modulus and argument of the complex number $\tilde{\chi}$. The amplitude has an attenuation factor given by $\mathrm{e}^{\mathrm{Im}(k)z}$.

The physical problem depends on a large number of parameters, each of them may vary in a quite wide range, and there is an enormous variety of different limiting cases. In the present work we will focus the attention on the influence of curvature – parametrized by ε – and letting all the others fixed. In the simulations, we take the following numerical parameters, referred to the vascular flow in a medium sized arterial segment:

$$\omega = 2\pi \text{ s}^{-1}, \quad a = 0.5 \text{ cm}, \quad h = 0.05 \text{ cm}, \quad E = 10^7 \text{ dyne/cm}^2,$$
$$\mu = 0.04 \text{ poise } \left(\text{g cm}^{-1}\,\text{s}^{-1}\right), \quad \rho = \rho_w = 1 \text{ g/cm}^3, \quad \sigma = 0.5,$$
$$A = 26000 \text{ dyne/cm}^2 \quad \left(\text{see Eq. (5.8)}\right),$$
$$\frac{\mathrm{d}\bar{p}_0}{\mathrm{d}z} = 7 \text{ dyne/cm}^3 \quad \text{(see Eq. (4.2))}.$$

With such parameters, the Womersley number is $\alpha = 6.266$ and the Dean number is

$$De_{\max} = \sqrt{2\varepsilon}\,\frac{d\bar{p}_0}{\mathrm{d}z}\frac{a^3\rho}{\mu^2} \approx 244.5,$$

corresponding to $\varepsilon_{\max} = 0.1$. The mesh size has been taken as $\Delta y = 0.02$.

A cross section of a curved tube with the inner wall at the left side is considered (Fig. 1). Either Eq. (7.1) or Eq. (7.2) are used to plot the flow pattern, the pressure distribution and wall deformations for a given time ($t = 0$) and a fixed axial coordinate ($z = 0$).

The effect of the curvature is examined by letting ε vary as $\varepsilon = 0, 0.05, 0.1$, and the corresponding amplitudes of the unsteady solution $\chi_0 + \varepsilon\chi_1$ are depicted in Fig. 2. Note that in a curved tube the solution becomes asymmetric and the degree of skewness (magnitude of secondary motion, location of peaks of axial velocity) increases with ε.

In Fig. 3, the transverse velocity in a curved tube is depicted in the section $z = 0$ and at time $t = 0$ for four values of curvature ε. It appears that the flow is axisymmetric for a straight tube ($\varepsilon = 0$), but lose the axisymmetric pattern as soon as $\varepsilon > 0$. In such regime a circulatory motion develops at the point where, in the axisymmetrical case, u_0 vanishes (Fig. 3 top right). Due to the centrifugal forces, such circulatory motion strengthens and the flow undergoes a transition with the closure of a vortex at the inner wall side (Fig. 3 bottom left).

For higher values of ε all the streamlines close, and such recirculating secondary flow pattern is approximately symmetrical about the line $\psi = 0$ and persists for larger curvature. The stagnation point stabilizes around a fixed point near the vertical axis and its location does not change with increasing ε.

To measure the strength of the secondary motion, an index given by the maximum modulus of the cross section velocity is introduced as $\Sigma = \max_{r,\psi}\sqrt{(\mathrm{Re}\,\tilde{u})^2 + (\mathrm{Re}\,\tilde{v})^2}$.

Another local indicator of the secondary flow is the vorticity having the following expression:

$$\Omega(y,\psi) = \frac{1}{ay}\left(\frac{\partial u}{\partial \psi} - v\right) - \frac{1}{a}\frac{\partial v}{\partial y}. \tag{7.3}$$

Being related to the flow field, Ω is sum of a steady part and a time dependent component:

$$\Omega = \overline{\Omega} + \widetilde{\Omega}(y,\psi)\,\mathrm{e}^{\mathrm{i}(\omega t - kz)}$$

and the amplitude $\widetilde{\Omega}$ is easily computed by combining the corresponding 0th and the 1st order expansions, namely:

$$\widetilde{\Omega}(y,\psi) = \widetilde{\Omega}^0 + \varepsilon\widetilde{\Omega}^1 = \varepsilon\widetilde{\Omega}^1 = \frac{\varepsilon}{a}\left(\frac{\breve{u}_1 - \breve{v}_1}{y} - \frac{\mathrm{d}\breve{v}_1}{\mathrm{d}y}\right)\cos\psi. \tag{7.4}$$

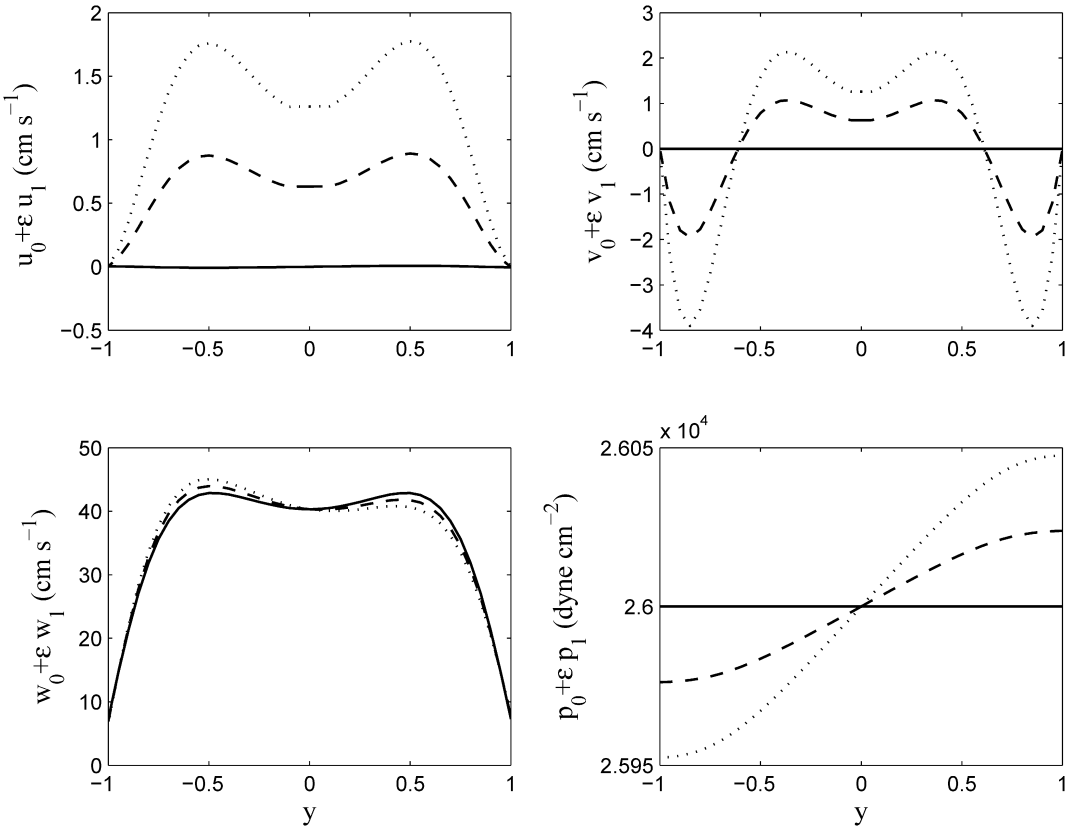

Fig. 2. Amplitude of the unsteady solution $\chi_0 + \varepsilon\chi_1$ for $\varepsilon = 0$ (continuous line), $\varepsilon = 0.05$ (dashed line) and $\varepsilon = 0.1$ (dotted line) along $[-1, 1]$.

It follows that, apart the dependence of ψ, the maximum of $\widetilde{\Omega}$ with respect to y is computed by searching the stationary points of the discrete function:

$$\widetilde{\Omega}^*(y_i, 0) = \frac{1}{a}\left(\frac{\breve{u}_1(y_i) - \breve{v}_1(y_i)}{y} - \frac{\breve{v}_1(y_{i+1}) - \breve{v}_1(y_i)}{\Delta y}\right). \tag{7.5}$$

$\widetilde{\Omega}^*$ shows a profile different than the correspondent vorticity of the steady flow. Moreover in the unsteady case, $\widetilde{\Omega}^*$ shows the evolution of the vorticity and the location of the stagnation points (see Fig. 9).

To understand the influence of the curvature on the axial velocity and pressure, the contour lines for $\tilde{p}_1$ and for $\widetilde{w}_1$ are depicted in Fig. 4. Note the boundary layer at $\psi = \pm\frac{\pi}{2}$, where a reversing of $\widetilde{w}_1$ takes place and the presence of an asymmetric flow in the full solution is evident (cf. Fig. 2) [5].

Wall shear stress τ: The two components of the wall shear stress are obtained from the flow field (see Eq. (2.3)) as:

$$\tau_\psi = (\boldsymbol{T}\boldsymbol{e}_r)\cdot\boldsymbol{e}_\psi = \frac{\mu}{a}\left(\frac{\partial v}{\partial y} - v + \frac{\partial u}{\partial \psi}\right)\bigg|_{y=1}$$

and

$$\tau_z = (\boldsymbol{T}\boldsymbol{e}_r)\cdot\boldsymbol{e}_z = \mu\left(\frac{1}{a}\frac{\partial w}{\partial y} + \frac{R\partial u/\partial z - w\sin\psi}{R + a\sin\psi}\right)\bigg|_{y=1}.$$

By neglecting the steady state component $\bar{\tau}$, the time dependent shear stress has a wave evolution similarly to the all the other variables (see Eqs. (3.4)):

$$\tau = \tilde{\tau}(\psi)\,\mathrm{e}^{\mathrm{i}(\omega t - kz)}$$

and the amplitudes $\tilde{\tau}$ are easily computed by summing up the 0th and the 1st order shear stresses, namely:

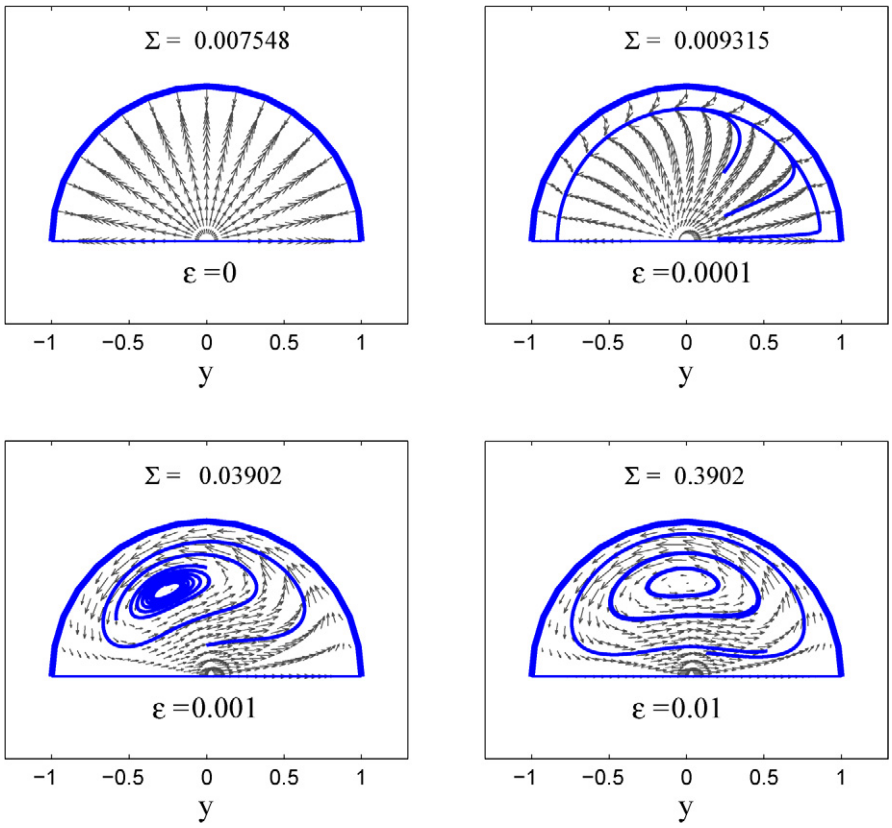

Fig. 3. Secondary flow $(\tilde{u}, \tilde{v})$ at $t = 0, z = 0$ in the upper cross-section of a curved tube for four values of ε. The maximum amplitude of the transverse velocity Σ is shown in each figure. For a critical $\varepsilon = \varepsilon_c \approx 4 \times 10^{-4}$ (top right) a recirculating flow starts to develop inwards and for $\varepsilon \geqslant \varepsilon_c$ moves inwards (bottom left). For an increasing ε the vortex stabilizes around a stagnation point located near the vertical diameter and the streamlines projected on the section appear closed (bottom right). A similar pattern is found at larger ε.

$$\tilde{\tau}_\psi = \tilde{\tau}_\psi^0 + \varepsilon\tilde{\tau}_\psi^1 = \varepsilon\tilde{\tau}_\psi^1 = \frac{\mu\varepsilon}{a}\left[\breve{u}_1 + \frac{\mathrm{d}\breve{v}_1}{\mathrm{d}y} - \breve{v}_1\right]_{y=1} \cos\psi, \tag{7.6}$$

$$\tilde{\tau}_z = \tilde{\tau}_z^0 + \varepsilon\tilde{\tau}_z^1 = \frac{\mu}{a}\left[\frac{d\widetilde{w}_0}{dy} + \varepsilon\left(\frac{\mathrm{d}\breve{w}_1}{\mathrm{d}y} - \breve{w}_0\right)\sin\psi\right]_{y=1}. \tag{7.7}$$

From Eq. (7.6) if follows that $\tilde{\tau}_\psi$ is present only in a curved tube and varies over a zero mean. Its maximum (resp. minimum) values are attained at $\psi = 0$ (resp. $\psi = \pi$). On the other hand, from Eq. (7.7), the axial wall shear stress $\tilde{\tau}_z$ varies over the correspondent value for the straight tube $\tilde{\tau}_z^0$ and its extrema are attained at to $\psi = \pm\frac{\pi}{2}$, in agreement with the boundary layer depicted in Fig. 4. Both of them vary linearly with ε, are opposite in sign, and the magnitude of the $\tilde{\tau}_\psi$ is smaller than $\tilde{\tau}_z$ (Fig. 5).

In Fig. 6, the pure oscillatory flow pattern in a curved elastic tube is shown at four instants. For the values of the parameters considered, a single vortex appears at most times, but a secondary clockwise vortex develops at the end of each half-cycle (see also Fig. 9). Contour lines for w are concentric circles and there are instants where the flow reverses. Plots at correspondent times in the second half-period show opposite values for w and the circulation reversed, while the value of Σ and the location of the vortices stay unchanged.

The structure of the secondary flow changes when the steady state solution is summed up (Figs. 7 and 8). The lowering of the primary vortex and the appearance of a second one of opposite sign detaching from the wall are clearly shown. Such double vortex structure, evidenced in other analytical and experimental works [5,26], is better characterized here and put in relation with the wall elasticity and the wave propagation characteristics. Axial velocity peak is shifted alternately inwardly and outwardly, and a flow reversal is displayed.

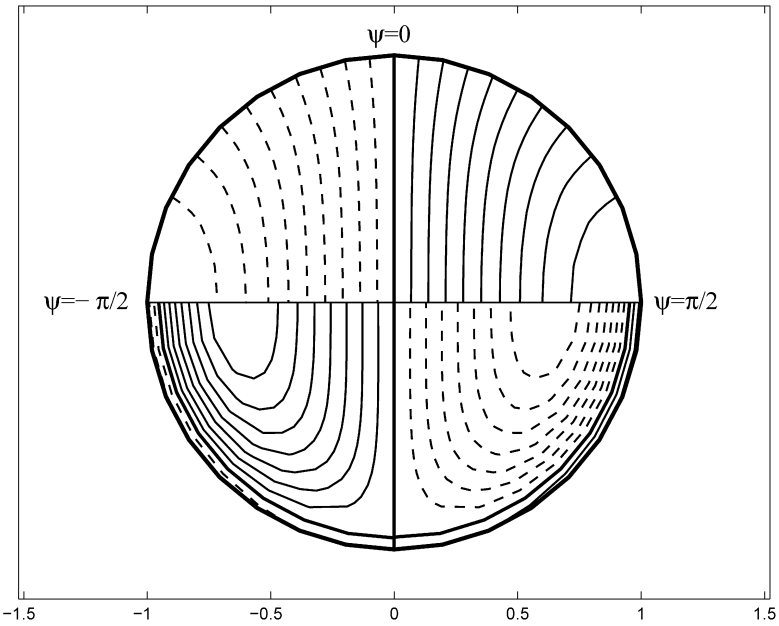

Fig. 4. Contour lines at equispaced levels for the first order solution in an half cross-section (continuous lines indicate positive levels, dashed lines negative levels, bold line zero levels). Pressure $\tilde{p}_1$ (half-top) and axial velocity $\tilde{w}_1$ (half-bottom) (cfr. Fig. 2). The 0th order pressure p_0 is constant on the cross section (see Eq. (5.8)), and the 0th order axial velocity w_0 is axisymmetric (see Eq. (5.10)).

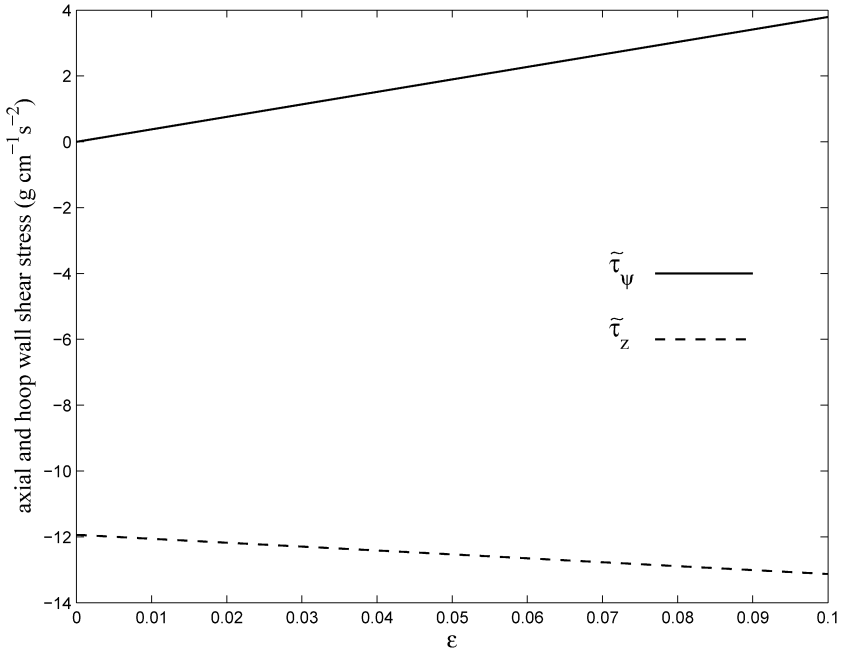

Fig. 5. Amplitude at $t = 0$, $z = 0$ of the axial ($\tilde{\tau}_z$) and hoop ($\tilde{\tau}_\psi$) wall shear stresses as functions of ε. The plots refer to the maximum values with respect to ψ.

Similarly to all the flow variables, the wall displacements are trigonometric functions of ψ (see Eq. (6.9)): as consequence $|\tilde{\eta}|$ and $|\tilde{\zeta}|$ are maximum at $\psi = \pm\frac{\pi}{2}$, while $|\tilde{\xi}|$ reaches its peaks at $\psi = 0$ and $\psi = \pi$ varying over their 0th order mean: the maximum displacement amplitudes (at $t = 0$, $z = 0$) are given in Table 1.

It is worth noting that $\tilde{\zeta}$ is at least one order of magnitude larger than $\tilde{\eta}$ and three order larger than $\tilde{\xi}$: this considerable high axial deformation disagrees with experiments reported in other studies which show $\tilde{\zeta}$ approximatively

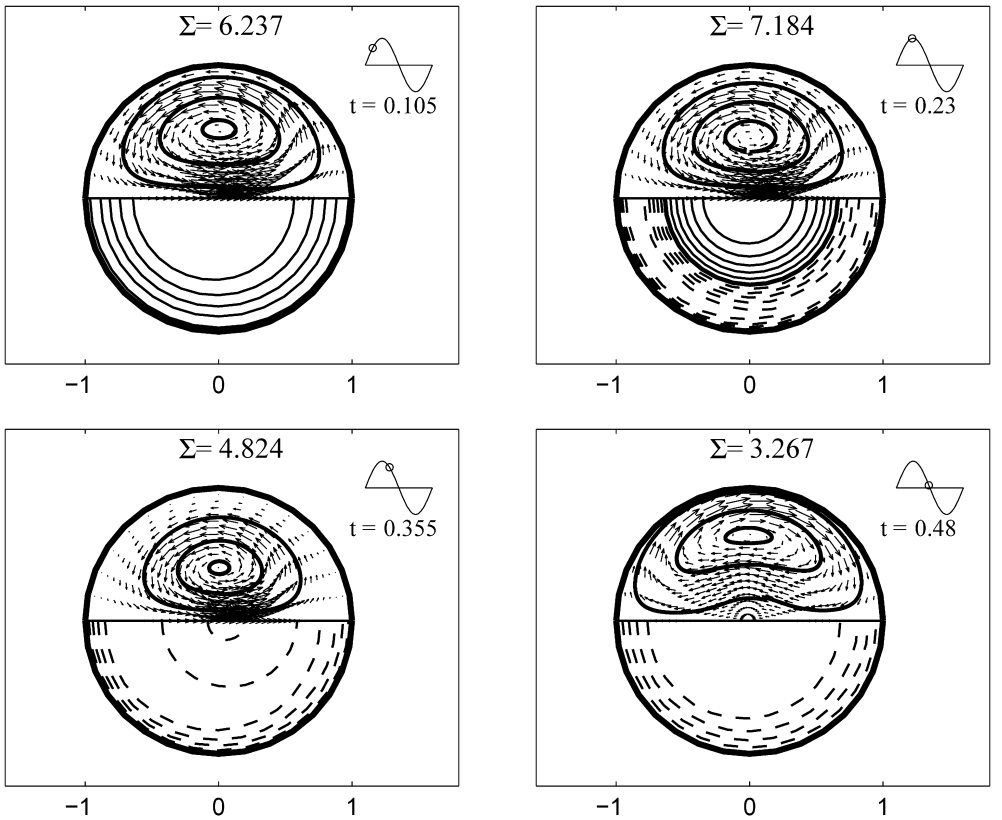

Fig. 6. Streamlines of secondary flow (above) and contour equispaced lines for axial velocity (below – continuous lines indicate positive levels, dashed lines negative levels, bold line zero levels) at four times in a half-period at $z = 0$. The plot refers to the unsteady solution $\tilde{\chi}\, \mathrm{e}^{\mathrm{i}(\omega t - kz)}$, with $\varepsilon = 0.1$.

zero [25]. This discrepancy can be avoided by considering a model with a tissue tethering effect as suggested in Ref. [25]. For a $E \lesssim 10^6$, the axial displacement amplitude becomes excessively large and this model is not consistent with the theory of linear elasticity and hence no longer representative.

Moreover, $k \simeq \mathrm{O}(\sqrt{1/E}\,)$, η and $\xi \simeq \mathrm{O}(1/E)$, while $\zeta \simeq \mathrm{O}(\sqrt{1/E}\,)$.

Wall tension:

It is of interest to analyze the wall tension components, given by:

$$
\begin{aligned}
S_{zz} &= \frac{Bh\sigma}{a}\left(\eta + \frac{\partial \xi}{\partial \psi}\right) + \frac{Bh}{R + a\sin\psi}\left(\eta \sin\psi + \xi\cos\psi + R\frac{\partial \zeta}{\partial z}\right),\\
S_{\psi z} &= Gh\left[\frac{1}{a}\frac{\partial \zeta}{\partial \psi} + \frac{1}{R + a\sin\psi}\left(R\frac{\partial \xi}{\partial z} - \zeta\cos\psi\right)\right],\\
S_{\psi\psi} &= \frac{Bh}{a}\left(\eta + \frac{\partial \xi}{\partial \psi}\right) + \frac{Bh\sigma}{R + a\sin\psi}\left(\eta \sin\psi + \xi\cos\psi + R\frac{\partial \zeta}{\partial z}\right)
\end{aligned}
\tag{7.8}
$$

(see Eq. (3.2)). Similarly to the shear stress components, the amplitudes of the unsteady wall tensions are:

$$
\begin{aligned}
\tilde{S}_{zz} = \tilde{S}^0_{zz} + \varepsilon\tilde{S}^1_{zz} &= \left(\frac{Bh\sigma}{a} + \omega^2\rho_w h\right)\eta_0 - \mathrm{i}Bhk\zeta_0\\
&\quad + \varepsilon\left[\frac{Bh}{a}\eta_0 + \mathrm{i}Bhk\zeta_0 + \left(\frac{Bh\sigma}{a} + \omega^2\rho_w h\right)\breve{\eta}_1 - \frac{Bh\sigma}{a}\breve{\xi}_1 - \mathrm{i}Bhk\breve{\zeta}_1\right]\sin\psi,
\end{aligned}
\tag{7.9}
$$

$$
\tilde{S}_{\psi z} = \tilde{S}^0_{\psi z} + \varepsilon\tilde{S}^1_{\psi z} = \omega^2\rho_w h\eta_0 + \varepsilon\left[Gh\left(-\frac{\zeta_0}{a} + \frac{\breve{\zeta}_1}{a} - \mathrm{i}k\breve{\xi}_1\right)\cos\psi + \omega^2\rho_w h\breve{\eta}_1\sin\psi\right],
\tag{7.10}
$$

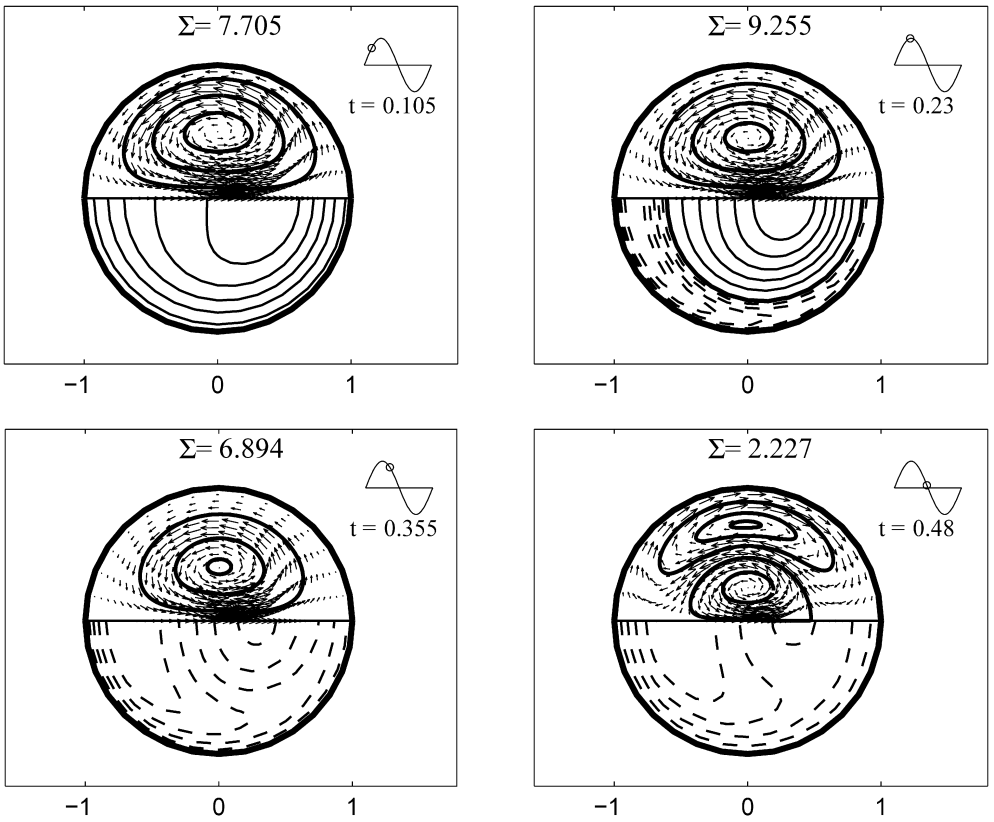

Fig. 7. Streamlines and secondary flow (above) and contour equispaced lines for axial velocity (below – continuous lines indicate positive levels, dashed lines negative levels, bold line zero levels) at eight times in a period at $z = 0$. The plot refers to the steady state solution summed up to unsteady solution $\bar{\chi} + \tilde{\chi}\,\mathrm{e}^{\mathrm{i}(\omega t - kz)}$, with $\varepsilon = 0.1$. A double vortex develops at the end of each half-cycle in correspondence of a small Σ.

$$\tilde{S}_{\psi\psi} = \tilde{S}^0_{\psi\psi} + \varepsilon \tilde{S}^1_{\psi\psi} = \left(\frac{Bh}{a} + \omega^2 \rho_w h\right)\eta_0 - \mathrm{i}Bh\sigma k\zeta_0 + \varepsilon\left[\frac{Bh\sigma}{a}\eta_0 + \mathrm{i}Bh\sigma k\zeta_0 + \left(\frac{Bh}{a} + \omega^2\rho_w h\right)\breve{\eta}_1 - \frac{Bh}{a}\breve{\xi}_1 - \mathrm{i}Bh\sigma k\breve{\zeta}_1\right]\sin\psi. \tag{7.11}$$

Note the different order of magnitude of $\tilde{S}_{zz}$ and $\tilde{S}_{\psi\psi}$ compared with $\tilde{S}_{\psi z}$. They vary linearly with ε and their extrema are attained at $\psi = \pm\frac{\pi}{2}$.

7.1. The limit case $E \to \infty$

When $E \to \infty$, it turns out that $k \to 0$, the wall tends to be rigid and the unsteady flow is damped out ($|\boldsymbol{v}| \to 0$). All the displacements tend to zero and the normal wall tensions to an asymptotic value (see Table 1). In such a limit case, the wave speed c and the wavelength λ both tend to be infinite.

Nevertheless, due to the absence of wall constraint, apart from the axisymmetry solution, another solution of the 0th order problem exists:

$$\begin{aligned} &u^*(\psi) = C\sin\psi, \qquad v^*(\psi) = C\cos\psi, \qquad w^* = 0, \qquad p^*(y,\psi) = -C\mathrm{i}\rho\omega a\sin\psi\, y, \\ &\eta^*(\psi) = -\frac{C}{\omega}\mathrm{i}\sin\psi, \qquad \xi^*(\psi) = -\frac{C}{\omega}\mathrm{i}\cos\psi, \qquad \zeta^* = 0 \end{aligned} \tag{7.12}$$

for any constant C. This solution is independent of the radial coordinate y (except the pressure that is linear in y) and represents a rigid motion with velocity C in the curvature plane. In other words, the fluid and the wall move jointly transversally as a rigid body and no travelling wave is present. Because of the axisymmetry condition, the translation

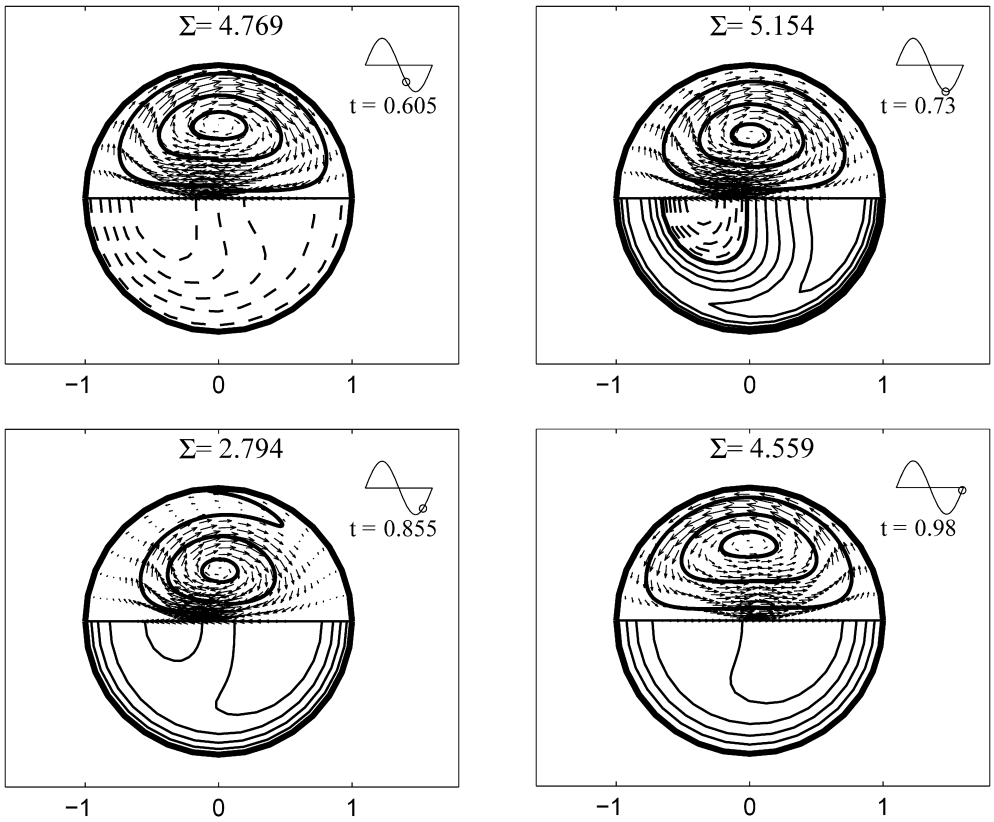

Fig. 8. Continuing of previous figure (same caption).

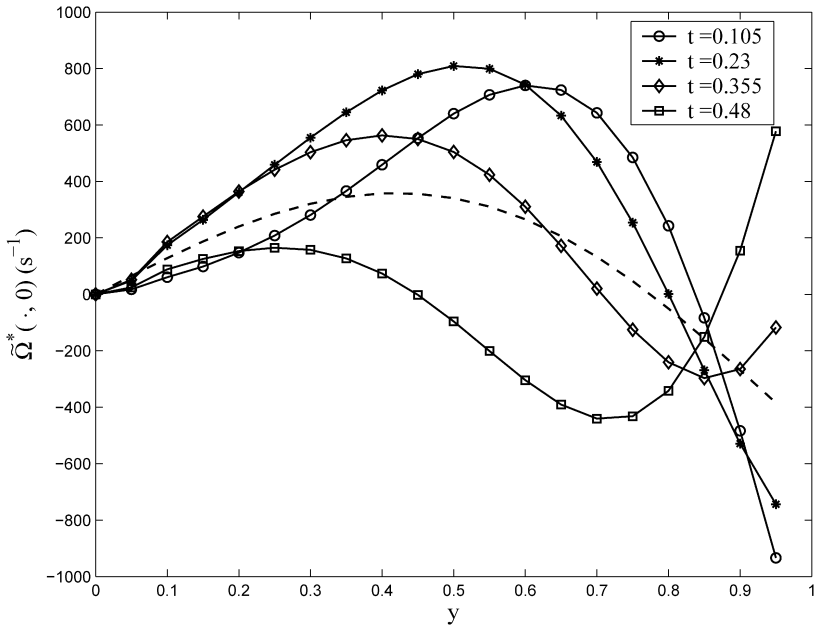

Fig. 9. Vorticity curves (see Eq. (7.5)) at four instants (as in Fig. 7) in an half-period ($z = 0$). Dashed line is the vorticity curve for the steady state solution. The stationary points of such curves indicate the location of the stagnation points and their values the strength and direction of vortices. The primary vortex moves at the center of the tube and, in the second quarter of the cycle a secondary vortex develops in the opposite direction from the wall. The magnitude of vorticity depends linearly on ε.

Table 1
Amplitudes of flow and wall variables at $t = 0$, $z = 0$ as function of the Young modulus E (with $\varepsilon = 0.1$). All the variables, except pressure and wall tensions, tend asymptotically to 0 as $E \to \infty$

–	$E = 5 \times 10^5$	$E = 10^7$	$E = 10^9$	$E = 10^{11}$	$E = 10^{13}$
k	0.0422	0.0095	9.45×10^{-4}	9.45×10^{-5}	9.45×10^{-6}
$\max_\psi \lvert\tilde{\eta}\rvert$	0.2349	1.172×10^{-2}	1.172×10^{-4}	1.172×10^{-6}	1.172×10^{-8}
$\max_\psi \lvert\tilde{\xi}\rvert$	0.00512	2.72×10^{-4}	2.76×10^{-6}	2.76×10^{-8}	2.76×10^{-10}
$\max_\psi \lvert\tilde{\zeta}\rvert$	1.7836	0.3988	0.0398	3.98×10^{-3}	3.98×10^{-4}
Σ	17.430	3.902	0.390	0.039	0.0039
$\max_{y,\psi} \lvert\tilde{w}\rvert$	200.64	45.061	4.511	0.451	0.0451
$\max_{y,\psi} \lvert\tilde{p}\rvert$	26213	26048	26005	26000	26000
$\max_y \lvert\widetilde{\Omega}^*(\cdot, 0)\rvert$	4234.67	946.80	94.675	9.4671	0.9467
$\max_\psi \lvert\tilde{\tau}_\psi\rvert$	16.93	3.787	0.378	0.037	0.0037
$\max_\psi \lvert\tilde{\tau}_z\rvert$	58.35	13.125	1.3146	0.1315	0.0131
$\max_\psi \lvert\tilde{S}_{zz}\rvert$	0.1839×10^4	0.1817×10^4	0.1810×10^4	0.1810×10^4	0.1810×10^4
$\max_\psi \lvert\tilde{S}_{\psi\psi}\rvert$	1.3961×10^4	1.3637×10^4	1.3648×10^4	1.3649×10^4	1.3649×10^4
$\max_\psi \lvert\tilde{S}_{\psi z}\rvert$	2.030	0.3971	0.0382	0.0041	0.0016

(7.12) is absent in the 0th order solution (see Section 5.1), but enters spuriously, smearing the first order solution, even for a finite values of E and becomes dominant as much as $E \to \infty$.

8. Conclusions

The unsteady flow of a viscous fluid in curved conduits has been studied by several authors. Although a number of areas of application are possible, the most relevant remains that of physiological flows, which provides the main motivation for this research.

On one hand the steady flow in a toroidal rigid tube has been the object of a thorough investigation by Dean. Most of the literature on flows in curved tubes refers to this basic work and concerns various extensions to the unsteady case, but is confined to rigid wall conduits. On the other hand, the classical works of Womersley shed light on the flow through an elastic straight tube and opened a series of subsequent studies on the characteristics of the wave propagation in arteries. In the present work a combined approach has been used to extend the theory of Womersley to an elastic curved tube in a comprehensive and consistent framework. In the paper of Chandran et al. [16], the problem has been faced with a model which includes wall tethering forces. However, the linearization process is hidden inside the perturbation expansion which is mixed up with the scaling procedure making it hard to separate the role and the influence of each single process.

In this work, the formulation starts from some basic principles of continuum mechanics and, under general assumptions, a formal complete procedure is clearly described and fully detailed to get the final form of the fluid–wall interaction model equations. In a wave propagation context, the dependence of the model on four independent parameters is outlined: the pressure amplitude A, the pulse frequency ω, the elasticity modulus E and the curvature parameter ε. In particular, the role of the latter is highlighted, and the character of the secondary flow addressed. All the scalar equations in this article have been derived anew with the aid of `Mathematica`®, starting directly from the basic equations in Section 2.

Some of the apparent limiting assumptions (wall isotropy, unconstrained tube, Newtonian fluid, fully developed flow) have been considered to make the model essential, and some others (small curvature, linearly elastic wall) are justified by the specific application. However, some restrictions can be removed, and the model can be extended in several directions.

Acknowledgement

The authors are grateful to L. Myers for stimulating the work and for his useful comments on this paper.

Appendix A

The fluid–structure interaction problem described in Section 2 in vector form is written in the toroidal coordinate system (r, ψ, θ) depicted in Fig. 1. The transformation from toroidal coordinates to Cartesian coordinates (x_1, x_2, x_3) is:

$$x_1(r,\psi,\theta) = (R + r\sin\psi)\cos\theta - R,$$
$$x_2(r,\psi,\theta) = (R + r\sin\psi)\sin\theta,$$
$$x_3(r,\psi,\theta) = r\cos\psi$$

where R the radius of curvature.

Fluid equations

Denoting by $\boldsymbol{v} = (u, v, w)$ the radial, the circumferential and the axial components of the fluid velocity respectively, the flow equations (2.6), (2.5) are written in scalar form as:

Continuity equation:

$$\frac{\partial u}{\partial r} + \frac{u}{r} + \frac{1}{r}\frac{\partial v}{\partial \psi} + \frac{u\sin\psi}{R + r\sin\psi} + \frac{v\cos\psi}{R + r\sin\psi} + \frac{1}{R + r\sin\psi}\frac{\partial w}{\partial \theta} = 0. \tag{A.1}$$

Flow equations:

$$\rho\left(\frac{\partial u}{\partial t} + u\frac{\partial u}{\partial r} + \frac{v}{r}\frac{\partial u}{\partial \psi} - \frac{v^2}{r} + \frac{w}{R + r\sin\psi}\frac{\partial u}{\partial \theta} - \frac{w^2\sin\psi}{R + r\sin\psi}\right)$$
$$= -\frac{\partial p}{\partial r} + \mu\left(\frac{\partial^2 u}{\partial r^2} + \frac{1}{r}\frac{\partial u}{\partial r} + \frac{1}{r^2}\frac{\partial^2 u}{\partial \psi^2} + \frac{\sin\psi}{R + r\sin\psi}\frac{\partial u}{\partial r} + \frac{1}{(R + r\sin\psi)^2}\frac{\partial^2 u}{\partial \theta^2} + \frac{\cos\psi}{r(R + r\sin\psi)}\frac{\partial u}{\partial \psi} - \frac{u}{r^2}\right.$$
$$\left. - \frac{u\sin^2\psi}{(R + r\sin\psi)^2} - \frac{2}{r^2}\frac{\partial v}{\partial \psi} - \frac{2v\sin\psi\cos\psi}{(R + r\sin\psi)^2} - \frac{vR\cos\psi}{r(R + r\sin\psi)^2} - \frac{2\sin\psi}{(R + r\sin\psi)^2}\frac{\partial w}{\partial \theta}\right), \tag{A.2}$$

$$\rho\left(\frac{\partial v}{\partial t} + u\frac{\partial v}{\partial r} + \frac{uv}{r} + \frac{v}{r}\frac{\partial v}{\partial \psi} + \frac{w}{R + r\sin\psi}\frac{\partial v}{\partial \theta} - \frac{w^2\cos\psi}{R + r\sin\psi}\right)$$
$$= -\frac{1}{r}\frac{\partial p}{\partial \psi} + \mu\left(\frac{\partial^2 v}{\partial r^2} + \frac{1}{r}\frac{\partial v}{\partial r} + \frac{1}{r^2}\frac{\partial^2 v}{\partial \psi^2} + \frac{2}{r^2}\frac{\partial u}{\partial \psi} + \frac{uR\cos\psi}{r(R + r\sin\psi)^2} + \frac{\sin\psi}{R + r\sin\psi}\frac{\partial v}{\partial r}\right.$$
$$\left. + \frac{1}{(R + r\sin\psi)^2}\frac{\partial^2 v}{\partial \theta^2} + \frac{\cos\psi}{r(R + r\sin\psi)}\frac{\partial v}{\partial \psi} - \frac{v}{r^2} - \frac{v\cos^2\psi}{(R + r\sin\psi)^2} - \frac{2\cos\psi}{(R + r\sin\psi)^2}\frac{\partial w}{\partial \theta}\right), \tag{A.3}$$

$$\rho\left(\frac{\partial w}{\partial t} + u\frac{\partial w}{\partial r} + \frac{v}{r}\frac{\partial w}{\partial \psi} + \frac{uw\sin\psi}{R + r\sin\psi} + \frac{vw\cos\psi}{R + r\sin\psi} + \frac{w}{R + r\sin\psi}\frac{\partial w}{\partial \theta}\right)$$
$$= -\frac{1}{R + r\sin\psi}\frac{\partial p}{\partial \theta} + \mu\left(\frac{2\sin\psi}{(R + r\sin\psi)^2}\frac{\partial u}{\partial \theta} + \frac{2\cos\psi}{(R + r\sin\psi)^2}\frac{\partial v}{\partial \theta} + \frac{\partial^2 w}{\partial r^2} + \frac{1}{r}\frac{\partial w}{\partial r} + \frac{1}{r^2}\frac{\partial^2 w}{\partial \psi^2}\right.$$
$$\left. + \frac{\sin\psi}{R + r\sin\psi}\frac{\partial w}{\partial r} + \frac{1}{(R + r\sin\psi)^2}\frac{\partial^2 w}{\partial \theta^2} + \frac{\cos\psi}{r(R + r\sin\psi)}\frac{\partial w}{\partial \psi} - \frac{w}{(R + r\sin\psi)^2}\right). \tag{A.4}$$

Wall equations. Let $\boldsymbol{u} = (\eta, \xi, \zeta)$ be the components of the wall displacement in the direction (r, ψ, θ) respectively. The three equations of the wall dynamics (see Eqs. (2.2)-(2.3)-(3.2)) are:

$$\rho_w h\frac{\partial^2 \eta}{\partial t^2} = \left[p - 2\mu\frac{\partial u}{\partial r}\right]_{r=a} - hB\left[\frac{\eta + \partial\xi/\partial\psi}{a^2} + \frac{\sin\psi\,(\eta\sin\psi + \xi\cos\psi + \partial\zeta/\partial\theta)}{(R + a\sin\psi)^2}\right]$$
$$- \sigma hB\left[\frac{\sin\psi\,(2\eta + \partial\xi/\partial\psi) + \xi\cos\psi + \partial\zeta/\partial\theta}{a(R + a\sin\psi)}\right], \tag{A.5}$$

$$\rho_w h\frac{\partial^2\xi}{\partial t^2} = -\mu\left[\frac{1}{a}\frac{\partial u}{\partial\psi} - \frac{v}{a} + \frac{\partial v}{\partial r}\right]_{r=a} + hB\left[\frac{\partial\eta/\partial\psi + \partial^2\xi/\partial\psi^2}{a^2} + \cos\psi\left(\frac{\eta + \partial\xi/\partial\psi}{a(R+a\sin\psi)} - \frac{\eta\sin\psi + \xi\cos\psi + \partial\zeta/\partial\theta}{(R+a\sin\psi)^2}\right)\right] + \sigma hB\left[\frac{-\xi\sin\psi + \sin\psi\,\partial\eta/\partial\psi + \partial^2\zeta/\partial\psi\partial\theta}{a(R+a\sin\psi)}\right] + hG\left[\frac{\partial^2\zeta/\partial\theta\partial\psi}{a(R+a\sin\psi)} + \frac{\partial^2\xi/\partial\theta^2 - \cos\psi\,\partial\zeta/\partial\theta}{(R+a\sin\psi)^2}\right], \tag{A.6}$$

$$\rho_w h\frac{\partial^2\zeta}{\partial t^2} = -\mu\left[\frac{1}{R+a\sin\psi}\frac{\partial u}{\partial\theta} - \frac{w\sin\psi}{R+a\sin\psi} + \frac{\partial w}{\partial r}\right]_{r=a} + hB\left[\frac{\sin\psi\,\partial\eta/\partial\theta + \cos\psi\,\partial\xi/\partial\theta + \partial^2\zeta/\partial\theta^2}{(R+a\sin\psi)^2}\right] + \sigma hB\left[\frac{\partial\eta/\partial\theta + \partial^2\xi/\partial\psi\partial\theta}{a(R+a\sin\psi)}\right] + hG\left[\frac{1}{a^2}\frac{\partial^2\zeta}{\partial\psi^2} + \frac{\partial^2\xi/\partial\psi\partial\theta + \zeta\sin\psi + \cos\psi\,\partial\zeta/\partial\psi}{a(R+a\sin\psi)} + \frac{\cos\psi\,\partial\xi/\partial\theta - \zeta\cos^2\psi}{(R+a\sin\psi)^2}\right]. \tag{A.7}$$

Interface conditions

Finally, the fluid–wall conditions (2.10) are imposed by requiring the matching of the fluid and wall velocities:

$$\frac{\partial\eta}{\partial t} = u|_{r=a}, \qquad \frac{\partial\xi}{\partial t} = v|_{r=a}, \qquad \frac{\partial\zeta}{\partial t} = w|_{r=a}. \tag{A.8}$$

References

[1] W.R. Dean, Note on the motion of fluid in a curved pipe, Philos. Mag. 4 (1927) 208–223.
[2] W.R. Dean, The stream line motion of fluid in curved pipes, Philos. Mag. 5 (1928) 673–693.
[3] M. Sankaraiah, Y.V.M. Rao, Analysis of steady laminar flow of an incompressible Newtonian fluid through curved pipes of small curvature, Trans. ASME I: J. Fluids Engrg. 95 (1973) 75–80.
[4] S.M. Barua, On secondary flow in stationary curved pipes, Quart. J. Mech. Appl. Math. 15 (1963) 61–77.
[5] W.H. Lyne, Unsteady viscous flow in a curved pipe, J. Fluid. Mech. 45 (1970) 13–31.
[6] R.G. Zalosh, W.G. Nelson, Pulsating flow in a curved tube, J. Fluid. Mech. 59 (1973) 693–705.
[7] T. Mullin, C.A. Greated, Oscillatory flow in curved pipes. Part 2, J. Fluid. Mech. 98 (1980) 397–416.
[8] F.T. Smith, Pulsatile flow in curved pipes, J. Fluid. Mech. 71 (1975) 15–42.
[9] D.M. Wang, J.M. Tarbell, Nonlinear analysis of oscillatory flow, with a nonzero mean, in an elastic tube (artery), J. Biomech. Eng. 117 (1995) 127–135.
[10] T.J. Pedley, The Fluid Mechanics of Large Blood Vessels, Cambridge Univ. Press, 1980 (Chapter 4).
[11] S.A. Berger, L. Talbot, L.S. Tao, Flow in curved pipes, Annu. Rev. Fluid Mech. 15 (1983) 461–512.
[12] C.C. Hamakiotes, S.A. Berger, Fully developed pulsatile flow in a curved pipe, J. Fluid. Mech. 195 (1988) 23–55.
[13] C.C. Hamakiotes, S.A. Berger, Periodic flows through curved tubes: the effect of the frequency parameter, J. Fluid. Mech. 210 (1990) 353–370.
[14] G. Pedrizzetti, Fluid flow in a tube with an elastic membrane insertion, J. Fluid Mech. 375 (1998) 39–64.
[15] M.W. Collins, G. Pontrelli, M.A. Atherton (Eds.), Wall–Fluid Interactions in Physiological Flows, Adv. Comput. Bioengin., vol. 6, WIT Press, 2004.
[16] K.B. Chandran, W.M. Swanson, D.N. Ghista, H.W. Yao, Oscillatory flow in thin-walled curved elastic tubes, Ann. Biomed. Eng. 2 (1974) 392–412.
[17] K.B. Chandran, R.R. Hosey, D.N. Ghista, V.W. Yao, Analysis of fully developed unsteady viscous flow in a curved elastic tube model to provide fluid mechanical data for some circulatory path-physiological situations and assist devices, J. Biomech. Eng. 101 (1979) 114–123.
[18] L.J. Myers, W.L. Capper, Analytical solution for pulsatile axial flow velocity waveforms in curved elastic tubes, IEEE Trans. Biomed. Engin. 48 (8) (2001) 864–873.
[19] J.R. Womersley, Oscillatory motion of a viscous liquid in a thin-walled elastic tube – I: The linear approximation for long waves, Philos. Mag. 46 (1955) 199–219.
[20] Y.C. Fung, A First Course in Continuum Mechanics, Prentice Hall Inc., 1977.
[21] L.D. Landau, E.M. Lifshitz, Fluid Mechanics, second ed., Pergamon Press, 1987.
[22] P. Le Tallec, J. Mouro, Fluid structure interaction with large structural displacement, Comput. Methods Appl. Mech. Engrg. 190 (2001) 3039–3067.
[23] W.R. Milnor, Hemodynamics, second ed., Williams and Wilkins, Baltimore, MD, 1989 (pp. 204–224, Chapter 8).

[24] C.A.J. Fletcher, Computational Techniques for Fluid Dynamics, vol. I, Springer-Verlag, 1997.
[25] J.R. Womersley, Oscillatory flow in arteries: the constrained elastic tube as a model of arterial flow and pulse transmission, Phys. Med. Biol. 2 (1957) 178–187.
[26] A.F. Bertelsen, L.K. Thorsen, An experimental investigation of oscillatory flow in pipe bends, J. Fluid. Mech. 118 (1982) 269–284.